SCIENTIFIC REPORTS

OPEN

A dye sensitized solar cell using natural counter electrode and natural dye derived from mangosteen peel waste

Received: 10 May 2015
Accepted: 14 September 2015
Published: 13 October 2015

Wasan Maiaugree[1], Seksan Lowpa[1], Madsakorn Towannang[1], Phikun Rutphonsan[1], Apishok Tangtrakarn[1,2,4], Samuk Pimanpang[1,2], Prapen Maiaugree[3], Nattawat Ratchapolthavisin[2], Wichien Sang-aroon[5], Wirat Jarernboon[1] & Vittaya Amornkitbamrung[1,2,4]

Mangosteen peel is an inedible portion of a fruit. We are interested in using these residues as components of a dye sensitized solar cell (DSSC). Carbonized mangosteen peel was used with mangosteen peel dye as a natural counter electrode and a natural photosensitizer, respectively. A distinctive mesoporous honeycomb-like carbon structure with a rough nanoscale surface was found in carbonized mangosteen peels. The efficiency of a dye sensitized solar cell using carbonized mangosteen peel was compared to that of DSSCs with Pt and PEDOT-PSS counter electrodes. The highest solar conversion efficiency (2.63%) was obtained when using carbonized mangosteen peel and an organic disulfide/thiolate (T_2/T^-) electrolyte.

Dye-sensitized solar cells (DSSCs) are a type of solar cell that has been intensively studied. Interest in DSSCs arises from their simple structure, low fabrication costs and promising efficiency in converting solar energy to electricity. This technology was first developed by O'Regan and Grätzel in 1991[1]. Three main components of a DSSC are the working electrode (WE), redox couple electrolyte (EL), and counter electrode (CE). Normally, the WE is composed of titanium dioxide attached with ruthenium complex dye (N719) coated upon a transparent conductive oxide. A triiodide/iodide (I_3^-/I^-) redox couple EL is normally used in DSSCs. Recently, an organic disulfide/thiolate (T_2/T^-) solution was used as an electrolyte in a DSSC to take advantage of this electrolyte's high transmittance and low corrosiveness[2,3]. Regarding the counter electrode material, Pt film is still widely used as a catalyst in DSSC devices. Unfortunately, use of Pt may not be a suitable option because of its high cost. To fabricate inexpensive solar cells, it is desirable to substitute low-cost catalytic materials for Pt. Such materials include carbon black[4], carbon nanotubes[5], graphite[6], graphene[7,8] and conductive polymers[9–12]. The catalytic activity of different carbon based electrodes was previously compared to Pt in T_2/T^- organic electrolyte. It was found that the catalytic activity of T_2/T^- match that of carbon based electrodes. Their surface areas are also high, therefore, the efficiency of carbon based DSSC was generally higher than Pt-DSSC's[13–15]. In addition, replacement of ruthenium complex compounds by natural dyes derived from wood, flowers or fruits are alternative ways to reduce costs of these cells. Natural pigments extracted from roselle, blue pea

[1]Department of Physics, Faculty of Science, Khon Kaen University, Khon Kaen 40002, Thailand. [2]Integrated Nanotechnology Research Center, Khon Kaen University, Khon Kaen 40002, Thailand. [3]Chumchon Ban Phon Ngam School, Akat Amnui District, Sakon Nakhon 47170, Thailand. [4]Nanotec-KKU Center of Excellence on Advanced Nanomaterials for Energy Production and Storage, Khon Kaen University, Khon Kaen 40002, Thailand. [5]Department of Chemistry, Faculty of Engineering, Rajamangala University of Technology Isan, Khon Kaen Campus, Khon Kaen 40000, Thailand. Correspondence and requests for materials should be addressed to V.A. (email: Vittaya@kku.ac.th)

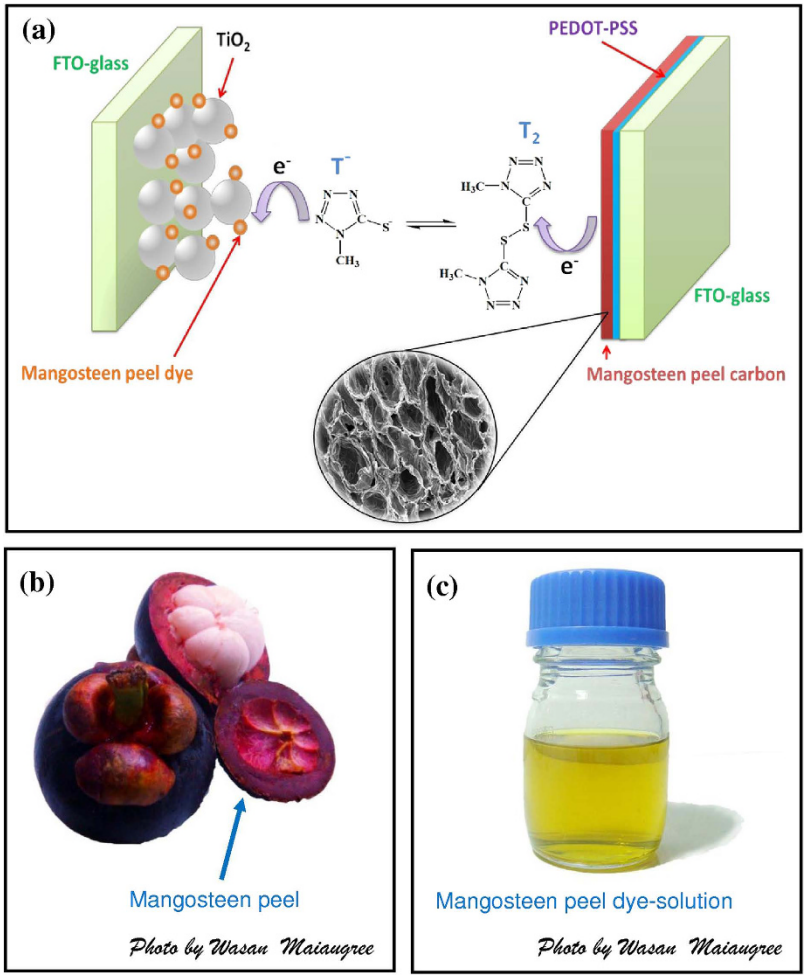

Figure 1. (**a**) The structure of mangosteen peel DSSC, (**b**) photograph of mangosteen (Photo by Wasan Maiaugree), and (**c**) mangosteen peel dye-solutions (Photo by Wasan Maiaugree).

flowers, shisonin, red Siahkooti fruit, red turnip and *Hibiscus surattensis* have been used as sensitizers in DSSCs. Unfortunately, all had solar to electric conversion efficiencies less than 2%[16–22]. However, there are reports of DSSCs sensitized using natural dyes attaining efficiencies exceeding 2%[23–25]. For example, Ito *et al.* used yellow pigment extracted from a *Monascus* (red rice) fermentation and reported an efficiency of 2.3%[26].

Mangosteen (*Garcinia mangostana L.*) is a tropical fruit in Southeast Asia, and is known as "the queen of fruit" in Thailand. The mangosteen peel instantly becomes waste after being consumed. In the current study, we fabricated the three components of a DSSC from organic materials. Both dye and counter electrode were prepared from waste mangosteen peel (the structure of mangosteen peel DSSC shows in Fig. 1a). In this report, we focused upon the effects of the wrinkled honeycomb-like structure and nanoscale rough surface of mangosteen peel carbon counter electrodes upon dye-sensitized solar cell performance. The resulting DSSC was easy to fabricate and showed promisingly efficiency of 2.6% for natural dyes.

Experimental

Preparation of dye solution. Dye derived from mangosteen was obtained in the following manner. Fresh mangosteen peels were milled and dried for 3–5 days at room temperature. A ten gram sample of mangosteen peel powder was soaked in 100 mL acetone (1:10 ratio) with stirring for 12 h at room temperature. The crude solution was filtered using Whatman No. 41 filter paper to remove solid residue. Finally, the concentrated dye solution was shielded from exposure to direct light and stored in a refrigerator at 5 °C.

Preparation of working electrode. TiO_2 film was prepared as previous reported[27]. Fluorine doped tin oxide on glass (FTO glass, 8Ω/sq, Solaronix) was used as a substrate. The FTO glass was treated with an aqueous solution of $TiCl_4$ (40 mM) at 70 °C for 30 min. Transparent and scattered TiO_2 films, each with an area of 0.25 cm^2, were coated on the $TiCl_4$ layer by a screen printing technique using TiO_2 pastes,

PST-18NR and PST–400 C, respectively (Catalysts & Chemicals Ind. Co., Ltd). The details of TiO_2 PST-18NR and TiO_2 PST–400 C are shown in supporting information (Fig. S1). TiO_2 films were annealed at 500 °C for 1 h then immersed in a concentrated dye solution for 24 h at room temperature.

Preparation of counter electrode. Dried mangosteen peels were carbonized at 850 °C for 2 h in an argon atmosphere. Pieces of mangosteen peel carbon (MPC) were cut into slices with dimensions of $0.4 \times 1.0 \times 0.02\,cm^3$. The slices of MPC were attached to FTO glass with10 μL of poly (3,4-ethylendioxythiophene)-poly (styrene sulfonate) (PEDOT-PSS). The MPCs attached to FTO glass were dried at ~80 °C for 6 h. A Pt counter electrode was prepared using a sputtering method and the PEDOT-PSS counter electrode was prepared using a drop casting method.

Preparation of electrolyte solution. Liquid organic T_2/T^- electrolyte was prepared from a mixture of 0.40 M $C_4H_6N_8S_2$ (T_2 (di-5-(1-methyltetrazole)), prepared as detailed in ref. 2, 0.40 M $C_6H_{15}N_5S$ ($NMe_4^+T^-$(5-mercapto-1-methyltetrazole N-tetramethylammonium salt)), prepared as detailed in ref. 2, 0.50 M TBP (4-tert-butylpyridine) and 0.05 M $LiClO_4$ (lithium perchlorate) in acetonitrile solvent.

The liquid I_2/NaI electrolyte was a mixture of 0.05 M iodide (I_2), 0.5 M sodium iodide (NaI) and 0.0025 M lithium carbonate (Li_2CO_3) in acetonitrile.

DSSC assembly. The DSSC was assembled using TiO_2 coated mangosteen peel dye sensitizer film as the working electrode and MPC, PEDOT-PSS or Pt films as the counter electrode. These two electrodes were assembled using a semi-closed DSSC method. The electrolyte was filled into the cells.

Film characterization. Film morphology was characterized using field emission scanning electron microscopy (FESEM; JEOL JSM-7001 F, Japan). Their structures were characterized using transmission electron microscopy (TEM) and selected area electron diffraction (SAED) (TECNAI G^2, the Netherlands), respectively. The surface area of mangosteen peel carbon was determined using a Brunauer–Emmett–Teller method (BET, Quantachrome AS-1, USA). The chemical bonding of MPC was investigated using a micro Raman triple spectrometer, Jobin Yvon Model T64000, equipped with a green argon ion laser (514.32 nm, 30 mW). A laser beam with a diameter of about 2 microns illuminated MPC with total scan time about 5 mins. This triple spectrometer has a spectral resolution of $\sim 0.15\,cm^{-1}$.

The electrical resistivities of films were determined using a four-point probe method (Keithley 617 Programmable Electrometer, USA) with Ag paste contacts. The film catalytic activity with T_2/T^- was measured using a cyclic voltammeter (CV, Gamry REF 3000, U.S.A) in a three-compartment cell with a scan rate 20 mV/s in 10 mM $NMe_4^+T^-$, 1 mM T_2 and 0.1 M $LiClO_4$ in an acetonitrile solution. A Pt plate and an Ag/AgCl electrode were used as a counter electrode and reference electrode, respectively. The cell performance was measured using a solar simulator (Peccell, PE-L111, Japan) system with a light intensity of $100\,mW{\cdot}cm^{-2}$. Incident photon-to-electron conversion efficiencies (IPCEs) of the devices under short-circuit conditions were determined with the aid of a Xe lamp (Oriel 150 W, USA) fitted with a monochromator (Cornerstone TM 130 1/8 m, USA) to provide a monochromatic light source. A silicon photodiode (Newport 818-UV, USA) was used for power density calibration with a picoammeter (Keithley 6485, USA). DSSC impedance was measured using electrochemical impedance spectroscopy (EIS, Gamry REF 3000, USA) under a light intensity $100\,mW{\cdot}cm^{-2}$ with frequency varied from 0.05 Hz to 100,000 Hz and an AC amplitude of 10 mV.

Results and Discussion

Figure 1b,c shows an optical image of mangosteen and concentrated dye solution extracted from mangosteen peel. A transparent yellow dye solution was obtained after filtration. The main components in the mangosteen peel extract were α-mangostin and anthocyanin derivatives[22,28–30]. The presence of these derivatives was revealed through their light absorption characteristics derived from UV-vis spectra. The absorbance spectra of solutions containing highly concentrated dye extended all the way from 350–680 nm (Fig. 2a) where the signature peak of chlorophyll was also found at 610 and 665 nm[31]. However, the absorption spectrum of mangosteen peel dye on TiO_2 showed absorption at wavelengths ranging from 350 to 550 nm. In this case, chlorophyll peak disappeared because there was little chlorophyll on TiO_2. Furthermore, a peak for α-mangostin was observed at around 350–370 nm[30,32] whilst anthocyanin derivative peaks were identified at ~440–460 nm[22] and 530–550 nm[31]. The α-mangostin and anthocyanin derivatives (Fig. 2b) extracted from various parts of different plants were previously tested as photosensitizers for DSSCs[22,33,34]. It is notable that the absorption spectrum of the dye-on-TiO_2 specimen was situated on a non-zero absorbance which belongs to TiO_2 nanoparticles. The non-zero absorbance of TiO_2 which occurs in Fig. 2a was assumed as an effect from a diffused reflection of suspending TiO_2 nanoparticles in solvent. Natural pigments can form bonds with the oxygen site of TiO_2 with the aid of carbonyl (C = O) and hydroxyl (O-H) groups[35–37]. Figure 2c illustrates how α-mangostin or anthocyanin could possibly bind with TiO_2. For α-mangostin, a possible anchoring mode is monodentate coordination via its available hydroxyl group whereas anthocyanin's possible anchoring mode is either by monodentate or bidentate bridging via its hydroxyl and carbonyl groups. For any successful bridging, when an incident photon is absorbed by α-mangostin and anthocyanin, electrons are promoted from a

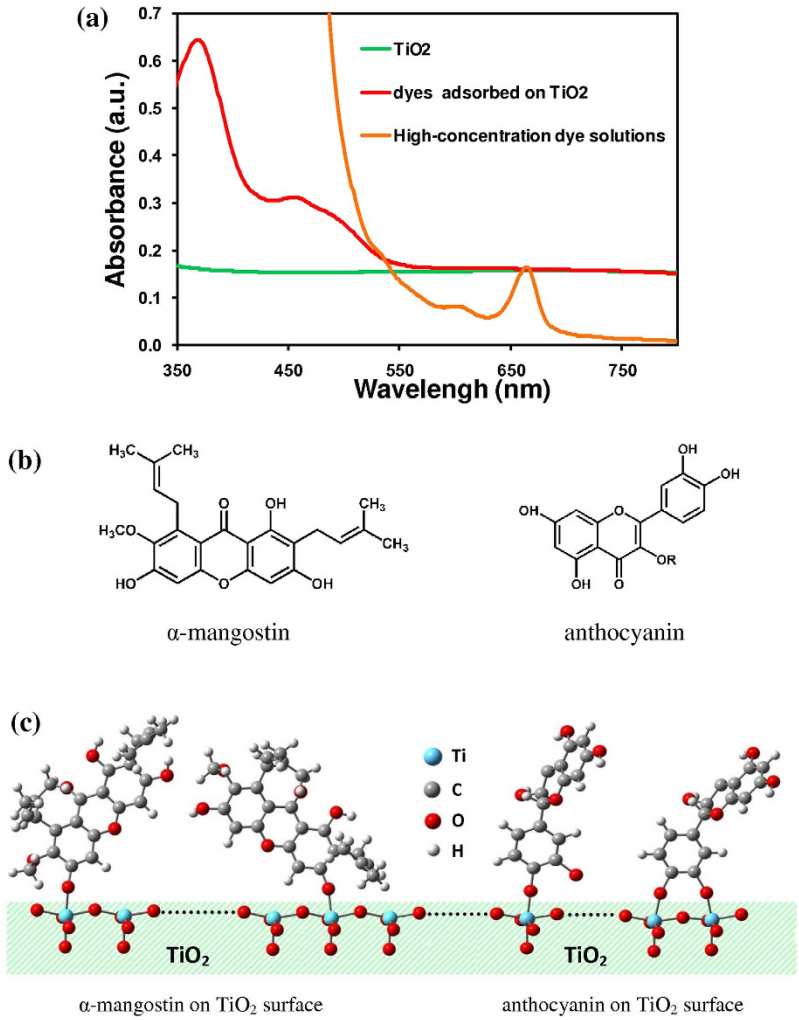

Figure 2. (**a**) The absorbance spectra of the mangosteen peel dye solutions, TiO_2 and the desorbed dye solutions of the TiO_2/Dye film in 5 ml of 0.1 M NaOH and ethanol at volume ratio of 1:1 and (**b**) structures of α-mangostin and anthocyanin and (**c**) possible binding schemes of α-mangostin and anthocyanin to TiO_2.

HOMO to LUMO state. Subsequently, the electron will be injected into the conduction band of the TiO_2 through functional anchoring groups.

Figure 3a shows images of Pt, PEDOT-PSS and MPC counter electrodes. The microstructure of MPC was characterized using FE-SEM and is shown in Fig. 3b,c. A honeycomb-like structure was observed with undulated walls as is seen in Fig. 3b. Moreover, the wall surface reveals some irregular nanoscale protrusions at high magnification as depicted in Fig. 3c. This created an unusually high interfacial area between the electrolyte and the counter electrode, which is excellent for DSSC applications. The thicknesses of MPC, Pt and PEDOT:PSS counter electrodes were 200 μm, 100 nm and 200 nm, respectively.

TEM images of MPC are presented in Fig. 4. MPC consists of graphite oxide nanosheets (Fig. 4a) and an amorphous carbon phase (Fig. 4c). The selected area electron diffractions of mangosteen peel carbon (Fig. 4b) are consistent with a graphite 2 H structure (JCPDF #751621) with the presence of (101), (110) and (112) planes. The enlargement of (002) d-spacing to 3.48 Å compared to that of graphite 2 H (3.40 Å), indicating the presence of graphite oxide. The amorphous part shows a diffuse diffraction pattern (Fig. 4d). The surface area of MPC was determined using a BET technique. MPC had 125 m^2/g of surface area, which is higher than that of a mesoscopic carbon electrode 91.08 $m^2.g^{-1}$ [34], glassy carbon (10 $m^2.g^{-1}$)[6], and graphite (10 $m^2.g^{-1}$)[6], but is a slightly lower than that of carbon black electrode (163.9 $m^2.g^{-1}$)[38], and much lower than graphite/carbon black (247.68 $m^2.g^{-1}$)[39] and activated carbon (2000 $m^2.g^{-1}$)[6]. Though increasing the surface area of the mangosteen peel can be done by chemical activation and could contribute to a further increase of the DSSC efficiency. Such attempt was not made here in order to avoid the use of harmful chemicals and to keep the fabrication steps as simple as possible. The pore distribution within MPC was determined by a Barrett-Joyner-Halenda method (BJH) and is shown in Fig. 5a. The effective pore size distributions of MPC were in the range of 1.15 nm to 15.76 nm, and the average pore

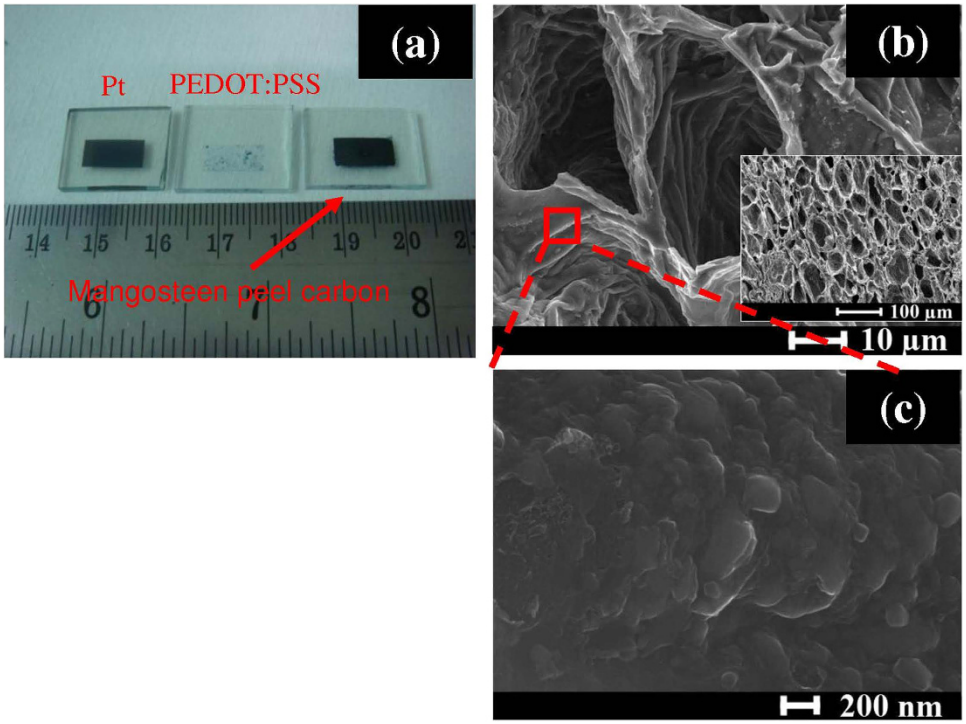

Figure 3. (**a**) Photograph of mangosteen peel carbon (MPC), PEDOT-PSS and Pt CEs, and (**b**,**c**) SEM images of mangosteen peel carbon (MPC).

size was about 1.49 nm. However, the surface area of Pt and PEDOT-PSS films could not be measured due to an insufficient supply of materials for the BET measurement.

Figure 5b shows Raman spectra of MPC. A broad D-peak (130.6 cm^{-1} of FWHM) was located at 1350 cm^{-1} which indicated the high disorder of sp3 carbon. The narrower G peak (68.8 cm^{-1} of FWHM) at 1595 cm^{-1} correlated with a graphite oxide phase, as indicated in previous published work[40]. From this information, it is clear that graphite oxide from MPC is a highly ordered sp2 hexagonal carbon oxide network.

The electrical resistivity (ρ) of PEDOT-PSS, MPC and Pt films on their glass substrates were measured using a four-point probe method. The results are given in Table 1. The electrical resistivity of PEDOT-PSS was 1.57×10^{-2} Ω•m and its electrical conductivity (σ) was 6.38×10 S/m. In the case of MPC and Pt films, low electrical resistivities of 1.72×10^{-4} Ω•m and 1.46×10^{-5} Ω•m were observed, respectively. Consequently, high σ values were observed, 5.81×10^{3} S/m for MPC and of 6.85×10^{4} S/m for Pt. This suggests that an electron can easily move from FTO glass to the front surface of the film (in contact with electrolyte).

The photocurrent density-voltage characteristics of MPC, PEDOT-PSS and Pt DSSCs based on T_2/T^- and I_2/NaI electrolytes are illustrated in Fig. 6. The photovoltaic performances of DSSCs are listed in Table 2. In the case of T_2/T^-, the MPC based DSSC had an open-circuit voltage (V_{OC}) of 0.60 V, a short-circuit current density (J_{SC}) of 8.70 mA·cm^{-2}, a fill factor (FF) of 0.50, and conversion efficiency (η) of 2.63%. In the case of the Pt based DSSC, values of V_{OC}, J_{SC}, FF and η were 0.57 V, 4.72 mA·cm^{-2}, 0.54 and 1.47%, respectively. Values of 0.58 V, 3.88 mA·cm^{-2}, 0.27 and 0.6% were observed for V_{OC}, J_{SC}, FF and η, respectively, for the PEDOT-PSS based DSSC. The short-circuit current density and conversion efficiency of MPC based DSSC were higher than those of the typical Pt and PEDOT-PSS based DSSCs. In the case of I_2/NaI electrolyte, the magnitude of performance values follows the order: MPC (1.99%) > Pt (1.75%) > PEDOT-PSS (0.88%). This trend is similar to T_2/T^- base electrolyte, but the highest efficiency (MPC-I_2/NaI) was lower than the efficiency of MPC-T_2/T^-. Therefore, we were interested only in organic T_2/T^- electrolyte. To confirm the effect of counter electrode type upon the DSSC performance, commercial N719 dye was used as a sensitizer in the working electrode and disulfide/thiolate was the redox couple electrolyte. DSSCs using N719 dye showed the same trend as the mangosteen peel dye DSSC. The details are shown in supporting information (Fig. S2 and Table S1).

To investigate the catalytic activity of the counter electrodes in the reduction of T_2, redox properties of the three electrodes were determined using cyclic voltammetry (CV). Figure 7 shows the CV curves of PEDOT-PSS, MPC electrodes and Pt electrodes. Two typical redox peaks were clearly observed for MPC and Pt electrodes, indicating high catalytic activity of T_2 reduction. A relative negative pair was associated with the reduction reaction of $T_2 + 2e^- \rightarrow 2T^{-3}$, whereas a positive peak was attributed to the oxidation reaction of $2T^- - 2e^- \rightarrow T_2$. It was found that the MPC counter electrode exhibited a higher

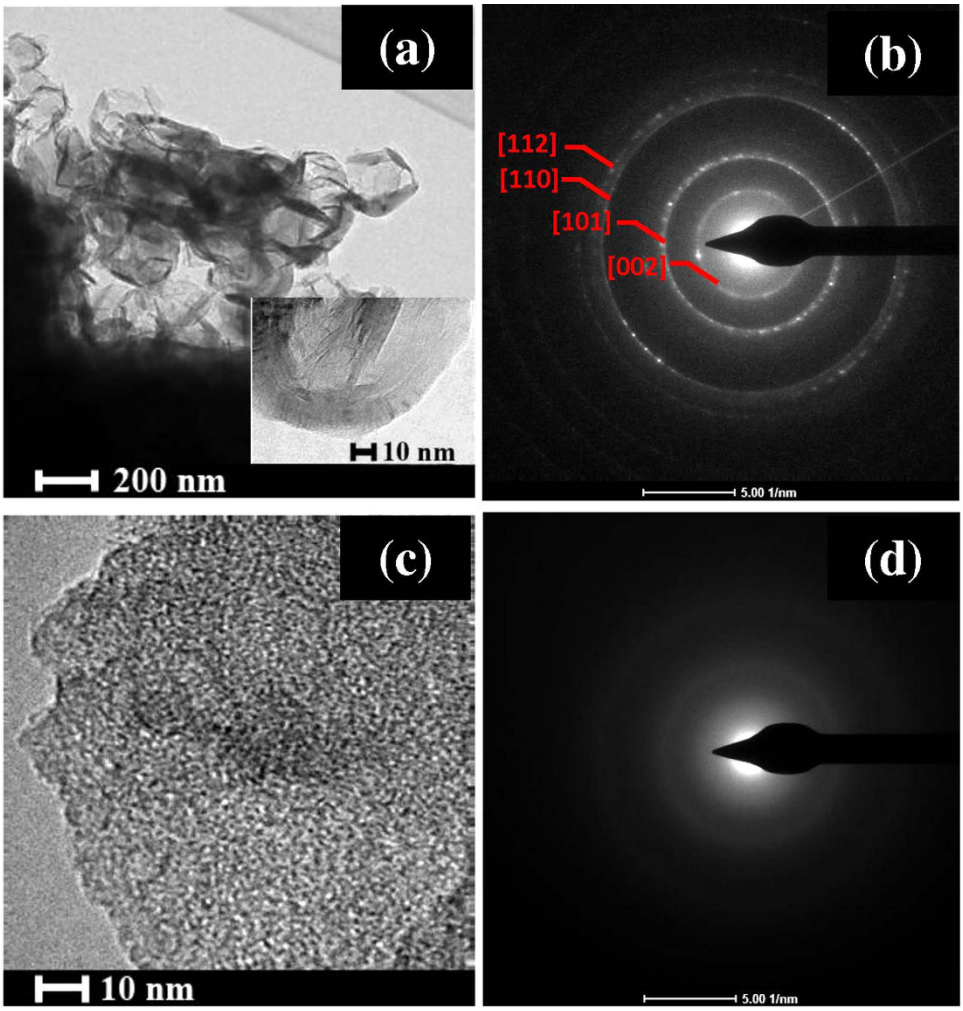

Figure 4. TEM images (**a**–**d**) and SAED patterns (e and f) of mangosteen peel carbon (MPC).

absolute current peak and more positive reduction peak potential than did the Pt and PEDOT-PSS counter electrodes. Moreover, the difference between the potential value of the oxidation peak and the reduction peak (ΔE_p) of Pt is 57 mV, whilst MPS's was 51 mV. Since ΔE_p was inversely correlated with the electron transfer rate constant (k_S), that is, a smaller ΔE_p indicates higher k_S[41,42]. Therefore, the MPC film manifested a faster reduction reaction rate in T_2 electrolyte. In comparison with another carbon-based counter electrode under the same conditions, the ΔE_p in current study was smaller than in another study based on annealed hydrothermal carbonized-glucose/TiC composite (59 mV)[43]. The excellent CV of MPC is likely due to its large surface area, PEDOT-PSS co-catalyst (binder) and mangosteen peel carbon. However, a poor redox reaction rate was observed for pure the PEDOT-PSS electrode in comparison to the MPC electrode. This indicated that the electrocatalytic activity of the MPC electrode can be attributed to MPC. Larger electrochemical-catalytic activity of MPC is advantageous for its efficient performance in the counter electrode of this DSSC device.

To reveal the electrochemical characteristics of DSSC counter electrodes, electrochemical impedance spectra (EIS) were measured in a symmetric cell configuration. This consisted of two identical counter electrodes (CEs). As shown in Fig. 8a, Nyquist plots of the CE–CE cells exhibit two semicircles. The semicircle in the high frequency region (left semicircle) is related to the charge-transfer resistance (R_{ct}) of the counter electrode/redox (T_2/T^-) electrolyte interface. The semicircle in the low frequency region (right semicircle) represents the Nernst diffusion impedance (Z_N) of the T_2/T^- redox couple within the electrolyte. The equivalent circuit of CE–CE cells obtained from fitting EIS spectra is shown in Fig. 9. R_{ct} is of primary interest as it represents the electron flow during the reduction of T_2 at the counter electrode. It is known that small resistance allows faster electron transfer rate, resulting in a higher solar cell performance. Larger resistance suppresses electron flow and causes low solar cell efficiency. In the case of the MPC symmetrical counter electrode, a small semicircle was observed in the high frequency region. The charge-transfer resistance of the MPC electrode (3.42 Ω) was lower than that of typical Pt (25.25 Ω) and PEDOT-PSS electrodes (152.25 Ω). This suggests that the MPC electrode has a superior electrocatalytic activity for the redox reaction of the T_2/T^- couple and a faster electron transport. These

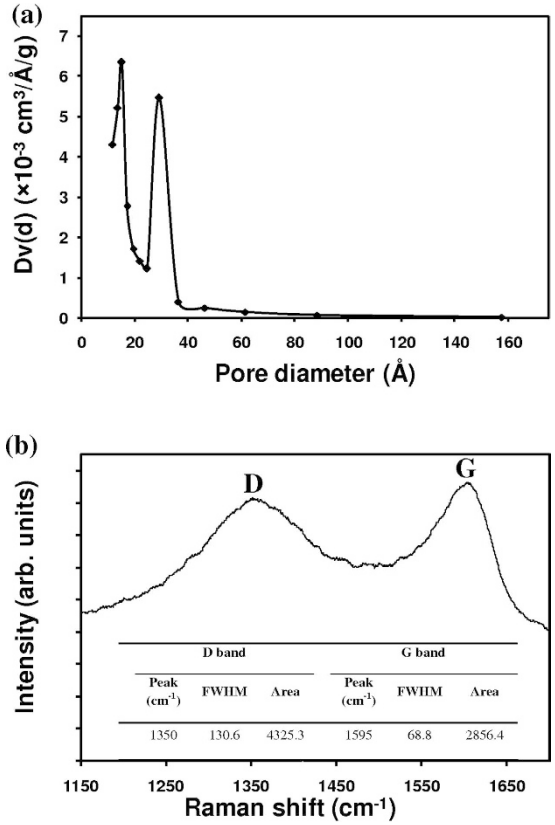

Figure 5. (**a**) Pore distribution and (**b**) Raman spectra of mangosteen peel carbon.

Counter electrode	Four-point probe		EIS of symmetric cells			EIS of DSSCs			
	ρ (Ω•m)	σ (S/m)	R_s (Ω)	R_{ct} (Ω)	C_μ (μF)	R_{s1} (Ω)	R_{ct1} (Ω)	f_{max} (Hz)	τ (ms)
PEDOT-PSS	1.57×10^{-2}	6.38×10	8.94	152.25	10.71	9.13	332.34	100	1.59
Pt	1.46×10^{-5}	6.85×10^{4}	8.15	25.25	11.28	8.24	19.50	126	1.26
MPC	1.72×10^{-4}	5.81×10^{3}	8.27	3.42	47.16	8.31	5.41	79	2.01

Table 1. Summary of electrical resistivity (ρ) and conductivity (σ) from a four-point probe, series resistance (R_s), charge-transfer resistance (R_{ct}), capacitance (C_μ) from symmetric cells, series resistance (R_{s1}) and charge-transfer resistance (R_{ct1}) at counter electrode/electrolyte, maximum frequency of the mid-frequency peak (f_{max}), electron lifetime (τ) of the DSSCs for mangosteen peel carbon (MPC), PEDOT-PSS and Pt DSSCs based on organic T_2/T^- electrolytes.

properties are important for improving the photovoltaic performance of the MPC based DSSC. The simulated chemical capacitance (C_μ) of the MPC electrode (47.16 μF) was significantly larger than that of the Pt electrode (11.28 μF). Provided that a counter electrode exhibits a capacitive property of an electrical double-layer capacitor[44], the capacitance value should related to the surface area of counter electrode. That is, a large electrochemical capacitance value of the electrode should relate to a large specific surface area, which is a crucial factor for high electrocatalytic activities[45–47]. In this study, an MPC electrode had a higher active surface area than that of sputtered Pt because its capacitance value was larger than Pt's. This is because the honeycomb-like features with nanoscale rough surfaces provide a large surface area in MPC electrodes. EIS of DSSCs was determined and is shown in Fig. 8b. Three semicircles were found in the EIS data for these DSSC devices. The high frequency region (left semicircle) represents the charge-transfer resistance at the counter electrode/electrolyte interface (R_{ct1}). The middle frequency region (middle semicircle) relates to the charge-transfer resistance at the working electrode/electrolyte interface (R_{ct2}). The low frequency region (right semicircle) represents the electrolyte diffusion resistance (Z_{N1}). The series resistance R_{s1}, R_{ct1} and R_{ct2} values of three counter electrodes are fitted and summarized in Table 1. It is seen that R_{ct1} of MPC based DSSC was 5.41 Ω, which is smaller than those of Pt based

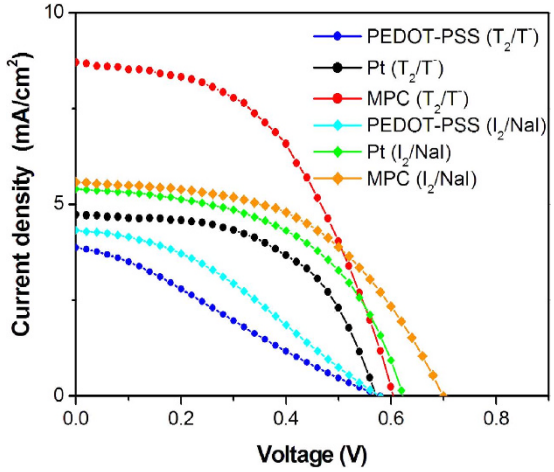

Figure 6. Photocurrent density (J) vs. photovoltage (V) curves of mangosteen peel carbon (MPC), PEDOT-PSS and Pt DSSCs based on T_2/T^- and I_2/NaI electrolytes.

Counter Electrode	Electrolyte	J_{SC} (mA cm^{-2})	V_{OC} (V)	FF	η (%)
Pt	T_2/T^-	4.72	0.57	0.54	1.47
PEDOT-PSS	T_2/T^-	3.88	0.58	0.27	0.60
Mangosteen peel carbon (MPC)	T_2/T^-	8.70	0.60	0.50	2.63
Pt	I_2/NaI	5.40	0.62	0.52	1.75
PEDOT-PSS	I_2/NaI	4.33	0.58	0.35	0.88
Mangosteen peel carbon (MPC)	I_2/NaI	5.58	0.70	0.51	1.99

Table 2. Photovoltaic characteristics of mangosteen peel dye DSSCs using different counter electrodes; open-circuit voltage (V_{oc}), short-circuit current density (J_{sc}), fill factor (FF) and solar cell efficiency (η).

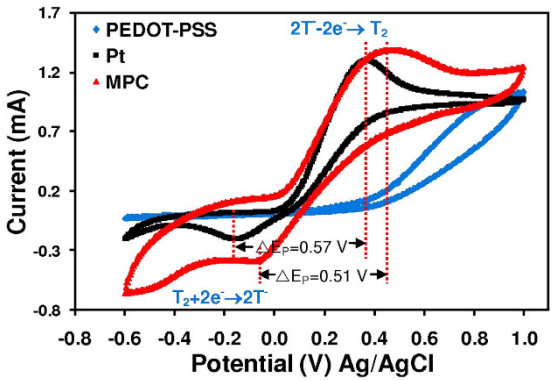

Figure 7. Cyclic voltammogram (CV) curves of mangosteen peel carbon (MPC), PEDOT-PSS and Pt electrodes at a scan rate of 20 mV/s in 10 mM $NMe_4^+T^-$, 1 mM T_2 and 0.1 M $LiClO_4$ in an acetonitrile solution.

DSSC (19.50 Ω) and PEDOT-PSS based DSSC (332.34 Ω). This result agrees well with the EIS outcomes of symmetrical CE-CE sets.

To confirm the validity of the J_{SC} trend derived from the I-V curve, the incident photon-to-collected electron conversion efficiencies (*IPCE*) were measured since J_{SC} is related to IPCE values according to Eq. 1:[48,49]

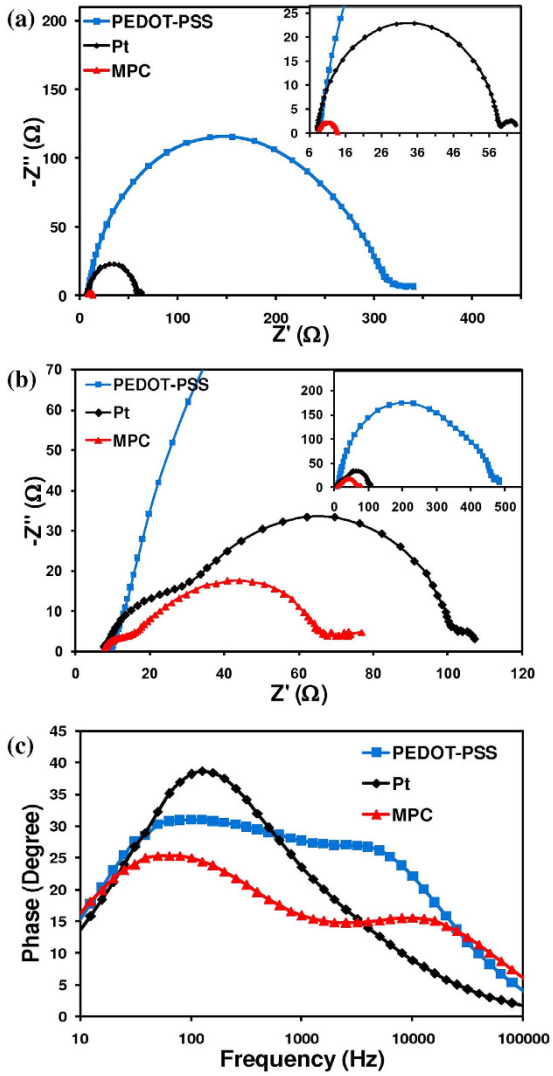

Figure 8. Nyquist plots of mangosteen peel carbon (MPC), and Pt electrodes for **(a)** symmetrical cell (CE-CE) **(b)** dye sensitized solar cells (DSSC) and **(c)** bode plot of DSSCs with MPC, PEDOT-PSS and Pt CE based on organic T_2/T^- electrolytes.

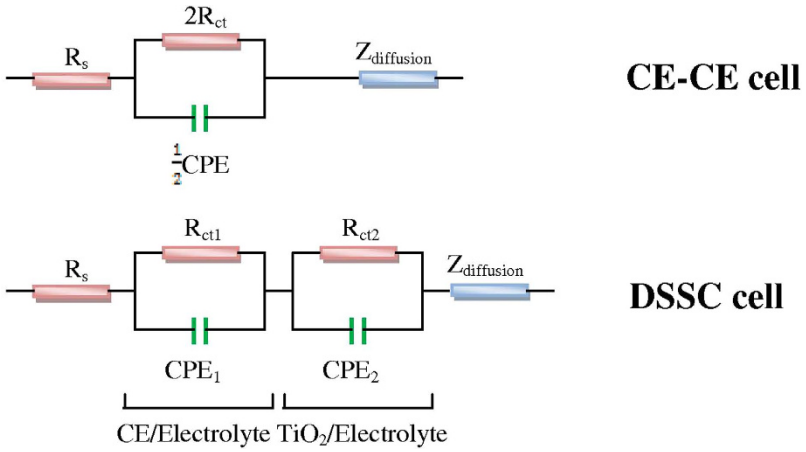

Figure 9. Schematic of (CE-CE) and DSSC equivalent circuit based on organic T_2/T^- electrolytes.

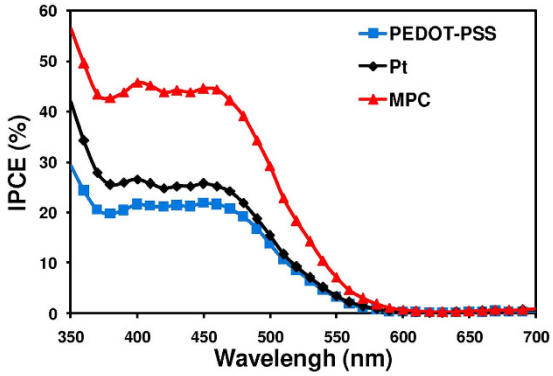

Figure 10. Incident photon-to-collected electron conversion efficiencies (IPCE) spectra of mangosteen peel carbon (MPC), PEDOT-PSS and Pt DSSCs based on organic T_2/T^- electrolytes.

$$J_{SC} = \int qF(\lambda)(1-r(\lambda))\,IPCE(\lambda)\,d\lambda \quad (1)$$

where $F(\lambda)$ is the incident photon flux density, q is the electronic charge and $r(\lambda)$ is the incident light loss in light absorption and reflection by the FTO-glass. The large IPCE(λ) was related to high J_{SC} in the DSSC. The IPCE spectra of the DSSCs based upon organic T_2/T^- electrolytes are shown in Fig. 10. The spectra present an effective absorption of mangosteen peel dye in comparison with other counter electrodes. All IPCE spectra were measured in wavelengths of 380–560 nm. The DSSC based upon a MPC counter electrode showed higher IPCE values than those of Pt and PEDOT-PSS based DSSCs. The maximum possible of J_{sc} values calculated from IPCE were 9.66 mA.cm^{-2} for MPC DSSC, 5.87 mA.cm^{-2} for Pt DSSC and 4.67 mA.cm^{-2} for PEDOT DSSC. This trend was similar to that of J_{sc} values obtained from the I-V curve.

The improvement of J_{SC} results from superior electron transportation at the counter electrode/electrolyte interfaces and good electrocalytic activity of MPC electrode. It is the key that leads to the high efficiency of the MPC based DSSC. The nanoscale roughness and honeycomb-like morphology of MPC electrode provide large surface area and high electrocatalytic activity for T_2/T^- redox reaction as evidenced in Figs 7 and 8a,b.

Conclusions

This work reports the preparation and photovoltaic performance of a natural organic- based DSSC. Dye extracted from mangosteen peel and carbonized mangosteen peel film were employed as a photosensitizer and a counter electrode catalyst, respectively. An organic disulfide/thiolate mixture was used as the electrolyte. SEM and TEM images show that mangosteen peel carbon counter electrode had a large active surface area due to its wrinkled honeycomb like structure with a nano-rough surface. The efficiency of the DSSC sensitized by mangosteen peel dye extract and mangosteen peel carbon counter electrode was 2.63%. This was higher than that of Pt counter electrode (1.47%). These results clearly show facile applications of a natural dye and carbon electrode derived from mangosteen peel as a photosensitizer and counter electrode in a DSSC. It shows promise for the realization of high performance from natural, low cost and environmentally friendly photovoltaic cells made from organic waste.

References

1. O'Regan, B. & Grätzel, M. A low-cost, high-efficiency solar cell based on dye-sensitized colloidal TiO 2 films. *Nature* **353,** 737–740 (1991).
2. Wang, M. *et al.* An organic redox electrolyte to rival triiodide/iodide in dye-sensitized solar cells. *Nat. Chem.* **2,** 385–389 (2010).
3. Wang, L., Wu, M., Gao, Y. & Tingli, M. Highly catalytic counter electrodes for organic redox couple of thiolate/disulfide in dye-sensitized solar cells. *Appl. Phys. Lett.* **98,** doi: 221102-221102-221103 (2011).
4. Kay, A. & Grätzel, M. Low cost photovoltaic modules based on dye sensitized nanocrystalline titanium dioxide and carbon powder. *Sol. Energy Mater. Sol. Cells* **44,** 99–117 (1996).
5. Suzuki, K., Yamaguchi, M., Kumagai, M. & Yanagida, S. Application of carbon nanotubes to counter electrodes of dye-sensitized solar cells. *Chem. Lett.* **32,** 28–29 (2003).
6. Imoto, K. *et al.* High-performance carbon counter electrode for dye-sensitized solar cells. *Sol. Energy Mater. Sol. Cells* **79,** 459–469 (2003).
7. Wang, H. & Hu, Y. H. Graphene as a counter electrode material for dye-sensitized solar cells. *Energ. Environ Sci.* **5,** 8182–8188 (2012).
8. Wang, H., Sun, K., Tao, F., Stacchiola, D. J. & Hu, Y. H. 3D Honeycomb-Like Structured Graphene and Its High Efficiency as a Counter-Electrode Catalyst for Dye-Sensitized Solar Cells. *Angew. Chem. Int. Ed.* **52,** 9210–9214 (2013).
9. Saito, Y., Kitamura, T., Wada, Y. & Yanagida, S. Poly(3,4-ethylenedioxythiophene) as a hole conductor in solid state dye sensitized solar cells. *Synth. Met.* **131,** 185–187 (2002).

10. Saito, Y., Kubo, W., Kitamura, T., Wada, Y. & Yanagida, S. I-/I3- redox reaction behavior on poly (3,4-ethylenedioxythiophene) counter electrode in dye-sensitized solar cells. *J. Photochem. Photobiol. A: Chem.* **164,** 153–157 (2004).
11. Li, Q. *et al.* Application of microporous polyaniline counter electrode for dye-sensitized solar cells. *Electrochem. Commun.* **10,** 1299–1302 (2008).
12. Muto, T., Ikegami, M. & Miyasaka, T. Polythiophene-based mesoporous counter electrodes for plastic dye-sensitized solar cells. *J. Electrochem. Soc.* **157,** B1195–B1200 (2010).
13. Ramasamy, E. *et al.* Soft-Template Simple Synthesis of Ordered Mesoporous Titanium Nitride-Carbon Nanocomposite for High Performance Dye-Sensitized Solar Cell Counter Electrodes. *Chem. Mater.* **24,** 1575–1582 (2012).
14. Liu, G. *et al.* An efficient thiolate/disulfide redox couple based dye-sensitized solar cell with a graphene modified mesoscopic carbon counter electrode. *Carbon* **53,** 11–18 (2013).
15. Xue, Y., Baek, J. M., Chen, H., Qu, J. & Dai, L. N-doped graphene nanoribbons as efficient metal-free counter electrodes for disulfide/thiolate redox mediated DSSCs. *Nanoscale* **7,** 7078–7083 (2015).
16. Wongcharee, K., Meeyoo, V. & Chavadej, S. Dye-sensitized solar cell using natural dyes extracted from rosella and blue pea flowers. *Sol. Energy Mater. Sol. Cells* **91,** 566–571 (2007).
17. Kumara, G. R. A. *et al.* Shiso leaf pigments for dye-sensitized solid-state solar cell. *Sol. Energy Mater. Sol. Cells* **90,** 1220–1226 (2006).
18. Mozaffari, S. A., Saeidi, M. & Rahmanian, R. Photoelectric characterization of fabricated dye-sensitized solar cell using dye extracted from red Siahkooti fruit as natural sensitizer. *Spectrochim. Acta Mol. Biomol. Spectros.* **142,** 226–231 (2015).
19. Calogero, G. *et al.* Efficient Dye-Sensitized Solar Cells Using Red Turnip and Purple Wild Sicilian Prickly Pear Fruits. *Int. J. Mol. Sci.* **11,** 254–267 (2010).
20. Fernando, J. M. R. C. & Senadeera, G. K. R. Natural anthocyanins as photosensitizers for dye-sensitized solar devices. *Curr. Sci.* **95,** 663–666 (2008).
21. Singh, L. K., Karlo, T. & Pandey, A. Performance of fruit extract of Melastoma malabathricum L. as sensitizer in DSSCs. *Spectrochim. Acta Mol. Biomol. Spectros.* **118,** 938–943 (2014).
22. Zhou, H., Wu, L., Gao, Y. & Ma, T. Dye-sensitized solar cells using 20 natural dyes as sensitizers. *J. Photochem. Photobiol. A: Chem.* **219,** 188–194 (2011).
23. Wang, X.-F., Zhan, C.-H., Maoka, T., Wada, Y. & Koyama, Y. Fabrication of dye-sensitized solar cells using chlorophylls c1 and c2 and their oxidized forms and from Undaria pinnatifida (Wakame). *Chem. Phys. Lett.* **447,** 79–85 (2007).
24. Ikegami, M., Ozeki, M., Kijitori, Y. & Miyasaka, T. Chlorin-sensitized high-efficiency photovoltaic cells that mimic spectral response of photosynthesis. *Electrochemistry* **76,** 140–143 (2008).
25. Wang, X. F. *et al.* Dye-sensitized solar cells using retinoic acid and carotenoic acids: Dependence of performance on the conjugation length and the dye concentration. *Chem. Phys. Lett.* **416,** 1–6 (2005).
26. Ito, S., Saitou, T., Imahori, H., Uehara, H. & Hasegawa, N. Fabrication of dye-sensitized solar cells using natural dye for food pigment: Monascus yellow. *Energ. Environ Sci.* **3,** 905–909 (2010).
27. Saekow, S., Maiakgree, W., Jarernboon, W., Pimanpang, S. & Amornkitbamrung, V. High intensity UV radiation ozone treatment of nanocrystalline TiO2 layers for high efficiency of dye-sensitized solar cells. *J. Non-Cryst. Solids* **358,** 2496–2500 (2012).
28. Du, C. T. & Francis, F. J. ANTHOCYANINS OF MANGOSTEEN, Garcinia mangostana. *J. Food Sci.* **42,** 1667–1668 (1977).
29. Palapol, Y. *et al.* Colour development and quality of mangosteen (Garcinia mangostana L.) fruit during ripening and after harvest. *Postharvest Biol. Technol.* **51,** 349–353 (2009).
30. Aisha, A. F. A. *et al.* Antitumorigenicity of xanthones-rich extract from garcinia mangostana fruit rinds on HCT 116 human colorectal carcinoma cells. *Braz. J. Pharmacog.* **21,** 1025–1034 (2011).
31. Noor, M. M. *et al.* Performance of Dye-Sensitized Solar Cells with (PVDF-HFP)-KI-EC-PC Electrolyte and Different Dye Materials. *Int. J. Photoenergy* **2011,** 5 (2011).
32. Ahmad, M., Yamin, B. M. & Lazim, A. M. Preliminary study on dispersion of α-mangostin in PNIPAM microgel system. *Malaysian Journal of Analytical Sciences* **16,** 256–261 (2012).
33. Buraidah, M. H. *et al.* TiO2/Chitosan-NH4I(+I2)-BMII-Based Dye-Sensitized Solar Cells with Anthocyanin Dyes Extracted from Black Rice and Red Cabbage. *Int. J. Photoenergy* **2011,** 11 (2011).
34. Cherepy, N. J., Smestad, G. P., Grätzel, M. & Zhang, J. Z. Ultrafast Electron Injection: Implications for a Photoelectrochemical Cell Utilizing an Anthocyanin Dye-Sensitized TiO2 Nanocrystalline Electrode. *J. Phys. Chem. B.* **101,** 9342–9351 (1997).
35. Zhang, L. & Cole, J. M. Anchoring Groups for Dye-Sensitized Solar Cells. *ACS Appl. Mater. Interfaces.* **7,** 3427–3455 (2015).
36. Hamadanian, M., Safaei-Ghomi, J., Hosseinpour, M., Masoomi, R. & Jabbari, V. Uses of new natural dye photosensitizers in fabrication of high potential dye-sensitized solar cells (DSSCs). *Mater. Sci. Semicond. Process.* **27,** 733–739 (2014).
37. Meng, S., Ren, J. & Kaxiras, E. Natural Dyes Adsorbed on TiO2 Nanowire for Photovoltaic Applications: Enhanced Light Absorption and Ultrafast Electron Injection. *Nano Lett.* **8,** 3266–3272 (2008).
38. Murakami, T. N. *et al.* Highly Efficient Dye-Sensitized Solar Cells Based on Carbon Black Counter Electrodes. *J. Electrochem. Soc.* **153,** A2255–A2261 (2006).
39. Xu, M. *et al.* Efficient monolithic solid-state dye-sensitized solar cell with a low-cost mesoscopic carbon based screen printable counter electrode. *Org. Electron.* **14,** 628–634 (2013).
40. Kudin, K. N. *et al.* Raman Spectra of Graphite Oxide and Functionalized Graphene Sheets. *Nano Lett.* **8,** 36–41 (2008).
41. Ramasamy, E. & Lee, J. Ferrocene-derivatized ordered mesoporous carbon as high performance counter electrodes for dye-sensitized solar cells. *Carbon* **48,** 3715–3720 (2010).
42. Hilmi, A., Shoker, T. A. & Ghaddar, T. H. Universal Low-Temperature MWCNT-COOH-Based Counter Electrode and a New Thiolate/Disulfide Electrolyte System for Dye-Sensitized Solar Cells. *ACS Appl. Mater. Interfaces.* **6,** 8744–8753 (2014).
43. Towannang, M. *et al.* High efficiency organic-electrolyte DSSC based on hydrothermally deposited titanium carbide-carbon counter electrodes. *Eelectron. Mater. Lett.*, 1–7 (2015).
44. Wu, M., Lin, X., Hagfeldt, A. & Ma, T. A novel catalyst of WO2 nanorod for the counter electrode of dye-sensitized solar cells. *Chem. Commun.* **47,** 4535–4537 (2011).
45. Maiaugree, W., Tangtrakarn, A., Lowpa, S., Ratchapolthavisin, N. & Amornkitbamrung, V. Facile synthesis of bilayer carbon/Ni3S2 nanowalls for a counter electrode of dye-sensitized solar cell. *Electrochim. Acta* **174,** 955–962 (2015).
46. Hauch, A. & Georg, A. Diffusion in the electrolyte and charge-transfer reaction at the platinum electrode in dye-sensitized solar cells. *Electrochim. Acta* **46,** 3457–3466 (2001).
47. Wu, M. *et al.* Economical and effective sulfide catalysts for dye-sensitized solar cells as counter electrodes. *Phys. Chem. Chem. Phys.* **13,** 19298–19301 (2011).
48. Lin, Y. H., Wu, Y. C. & Lai, B. Y. Collection efficiency enhancement of injected electrons in dye-sensitized solar cells with a Ti interfacial layer and TiCl4 treatment. *Int. J. Electrochem. Sci.* **7,** 9478–9487 (2012).
49. Wang, Z.-S., Kawauchi, H., Kashima, T. & Arakawa, H. Significant influence of TiO2 photoelectrode morphology on the energy conversion efficiency of N719 dye-sensitized solar cell. *Coord. Chem. Rev.* **248,** 1381–1389 (2004).

Acknowledgements

This work was supported by the Thailand Research Fund through the Royal Golden Jubilee Ph.D. Program (PHD/0080/2554), the Nanotechnology Center (NANOTEC), NSTDA, Ministry of Science and Technology, Thailand, through its program of Center of Excellence Network, Center for Alternative Energy Research and Development, Khon Kaen University, the Integrated Nanotechnology Research Center, Khon Kaen University, the Higher Education Research Promotion and National Research University Project of Thailand, Office of the Higher Education Commission, through the Advanced Functional Materials Cluster of Khon Kaen University, the Thailand Center of Excellence in Physics, CHE, Ministry of Education, Bangkok, and Energy Policy and Planning Office, Ministry of Energy, Bangkok, Thailand.

Author Contributions

W.M. and V.A. wrote the main manuscript text. S.L., M.T. and P.R. prepared figures 2–5. P.M. and N.R. prepared figures 6–9. A.T., S.P., W.S. and W.J. reviewed and commented the manuscript.

Additional Information

Supplementary information accompanies this paper at http://www.nature.com/srep

Competing financial interests: The authors declare no competing financial interests.

How to cite this article: Maiaugree, W. *et al.* A dye sensitized solar cell using natural counter electrode and natural dye derived from mangosteen peel waste. *Sci. Rep.* **5**, 15230; doi: 10.1038/srep15230 (2015).